A Novel Method for Rotor Tracking Using Bipolar Electrogram Phase

Caroline H Roney, Chris D Cantwell, Jennifer H Siggers, Fu Siong Ng, Nicholas S Peters

Imperial College London, London, UK

Abstract

Assessing the location and stability of electrical rotors can help target ablation therapy for atrial fibrillation. Rotor cores can be tracked by identifying singularities in the phase of spatially distributed electrical recordings. This is routinely applied to unipolar electrogram and action potential data, but not to bipolar electrogram data, which contains local activation only. We developed and tested a technique to track phase singularities from simulated bipolar data. Bipolar electrogram phase was found to be as effective as action potential and as unipolar electrogram phase for rotor tip detection when using simulated data, suggesting that it may be used clinically as an alternative method to unipolar phase to locate rotor phase singularities in atrial fibrillation.

1. Introduction

Atrial fibrillation (AF) is the most prevalent cardiac arrhythmia and there are multiple hypotheses for its mechanistic basis. One proposal is the mother rotor hypothesis, which states that AF is not entirely random, but is perpetuated in a hierarchical manner by periodic rotors that act as sources of high frequency wavefronts, driving fibrillation. Despite the presence of rotors in animal experimental studies [1], little evidence had been found for the existence of rotors in humans [2] until the recent development of different clinical computational mapping modalities that successfully identified rotors and focal sources in the atria [3,4]. These studies suggest that assessing the location and stability of rotors can help target ablation therapy for AF.

Fibrillatory electrograms are challenging to analyse due to their beat-to-beat variability in amplitude and duration, and fibrillation itself being a seemingly random process. However, the periodicity in the signal can be translated into attractors in its phase space, leading to spatial singularities in phase corresponding to the centre of a rotating wave [5]. Identifying phase singularities (PS) is one approach that can be used to locate the tip of spiral waves.

Phase mapping was initially developed for optical mapping data, where the fluorescence signal was plotted against a time-shifted signal to reveal attractors, and the phase angle parameterises the trajectory, giving a representation that is independent of the changing amplitude and morphology of the signal. PSs occur at the ends of wavefronts, including at centres of rotational activity, and can be tracked over time to investigate wave dynamics. Many optical mapping and simulation studies have since used these techniques to analyse wavefront dynamics from action potential (AP) data [6].

More recently phase mapping using unipolar electrograms has been applied to ventricular fibrillation [7] and AF data [4]. Bipolar electrogram signals have the advantage that they contains local activation only. In this paper, we describe a technique to track PSs from simulated bipolar electrogram data, at various inter-electrode spacings to assess its theoretical suitability for use in a clinical environment. Computed wavefront dynamics and singularity positions, are compared to those calculated from AP data and unipolar electrogram data.

2. Methods

Data for testing the algorithms were generated from a simulation initiated with two fixed rotors on a 10cm $\times$10cm two-dimensional domain, Ω. The monodomain tissue model and the Courtemanche *et al.* human atrial cell model [8] were used; electrical remodelling in AF was represented by reducing the ionic conductances of I_{to}, I_{Kur} and I_{CaL} [9]. In addition, the conductance of I_{K1} was doubled on one side of the domain, reducing the action potential duration (APD) [10], and allowing rotors with two different frequencies to be established. A smooth transitional region was included along the centre of the domain. The model was discretised using finite differences with a 0.1mm resolution. Voltages and ionic concentrations were time-marched using forward Euler and gating variables were advanced using a Rush-Larsen scheme [11], both with a time-step of 0.01ms.

An electrogram at a point (x_p, y_p, z_p) is calculated as:

$$\Phi_e(x_p, y_p, z_p) = D \int \int_{\Omega} \nabla V_m \cdot \nabla \left(\frac{1}{R} \right) \mathrm{d}x \, \mathrm{d}y, \quad (1)$$

where $R = \sqrt{(x-x_p)^2 + (y-y_p)^2 + (z-z_p)^2}$ is the distance from the electrode [12], D is the diffusion co-

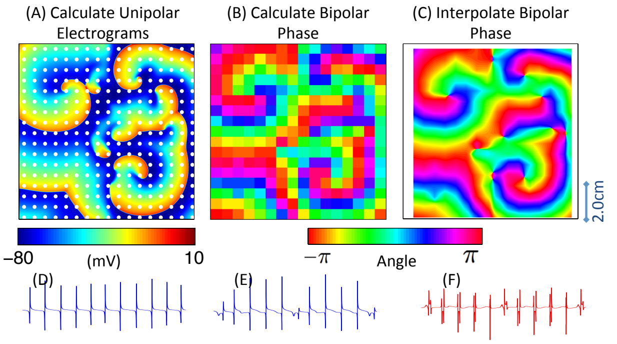

Figure 1. Summary of data modalities. (A) AP data was post-processed to derive unipolar electrograms at the white dots, with 6mm inter-electrode spacing. (B) These were paired to give bipolar electrograms and the phase was calculated. (C) Phase interpolated to the original grid resolution. (D, E) Example unipolar electrograms paired to give bipolar electrogram (F).

efficient and V_m is the membrane potential. Unipolar electrograms were measured on a regular grid (Fig. 1A), one cell radius (5μm) above Ω. Bipolar electrograms were calculated as the difference of two unipolar electrograms (Figs. 1D-1F).

Bipolar electrograms were calculated at inter-electrode spacings of 2, 4, 6, 8 and 10mm. Filtering was applied using the sequence of filters suggested by Ng *et al.* for dominant frequency analysis [13]: a band-pass filter from 40–250Hz; rectification of the signal; and a low-pass filter at 20Hz. Signals for large inter-electrode spacings ($>$ 4mm) were treated differently; a 10Hz low-pass filter was used to reduce the number of double potentials.

2.1. Phase Calculation

To identify rotor cores and track wavefront dynamics, we calculated the phase of the voltage signal (either AP, unipolar electrogram or bipolar electrogram). A signal with zero-mean was necessary to correctly compute the phase angle. For small electrode spacings, a piecewise cubic hermite polynomial spline was fitted to the maxima in the signal. This was used to normalise the signal, and subsequently a straight mean was removed (Figs. 2A and 2B). For large electrode spacings, a slightly different approach was used. Maxima were assigned using a window size of 70ms and the minima between each pair of maxima were also tagged. Maxima-minima pairs for which the amplitude difference was small were deleted, and the maxima were temporally shifted to be centred between adjacent minima. The maxima and minima points were again joined using splines, and used to normalise the signal. This signal was then squared and finally the overall mean was removed. In both cases, the real and imaginary parts of

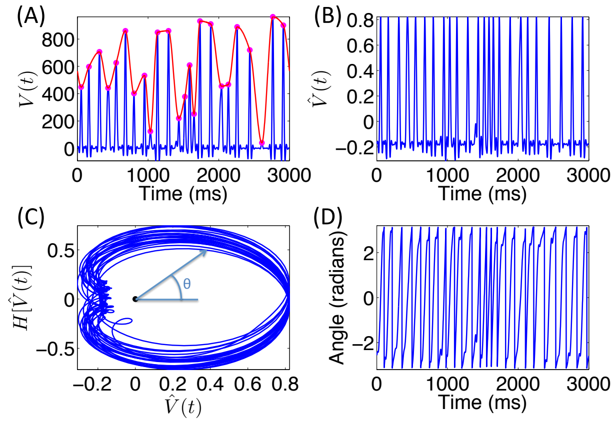

Figure 2. Calculation of bipolar electrogram phase with 2 or 4mm interelectrode spacing. (A) Tagged maxima, joined using a cubic spline. (B) Signal after normalisation using the maxima line and with straight mean removed. (C) Real and imaginary parts of the Hilbert-transformed signal plotted in the phase plane. (D) Phase angle.

the Hilbert transform of the zero-mean signal were plotted in the phase plane (Fig. 2C) [14], and the angle around this trajectory was the phase angle (Fig. 2D). This was displayed as a spatial map of phase (Fig. 1B), which was then interpolated to the original resolution (Fig. 1C). Similar techniques were used to calculate the AP phase and unipolar electrogram phase.

PSs are locations where the phase is considered arbitrary or undefined, and a 2π increase in phase is seen in the surrounding points. A PS is defined as a site where the integral of the topological charge is non-zero:

$$n_t \equiv \frac{1}{2\pi}\oint_c \nabla\theta \cdot \mathrm{d}\mathbf{r} = \pm 1.$$

To calculate this integral, we used the technique given in Bray and Wikswo [15]. PS locations calculated using the AP data were used when assessing the capabilities of the bipolar algorithms.

3. Results

The left-hand side of the domain maintains a single isolated rotor throughout the simulation, without the presence of wavefront collisions, and so is used to assess the accuracy of PS identification. The location of the PS corresponding to this rotor was extracted for each frame of the simulation. Fig. 3 shows the rotor core trajectories calculated at a fixed inter-electrode spacing of 2mm for the different signals. Each of the trajectories are seen, to some extent, to align with the 2mm grid. The trajectory calculated from the full-resolution data is also shown for comparison.

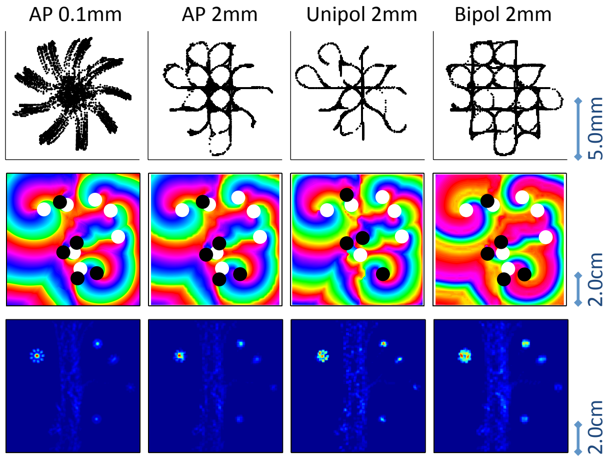

Figure 3. Top: Isolated rotor trajectories. Middle: PSs (black and white dots) calculated using full resolution AP phase; and AP phase, unipolar phase and bipolar electrogram phase generated at 2mm inter-electrode spacings. Bottom: PS heat maps.

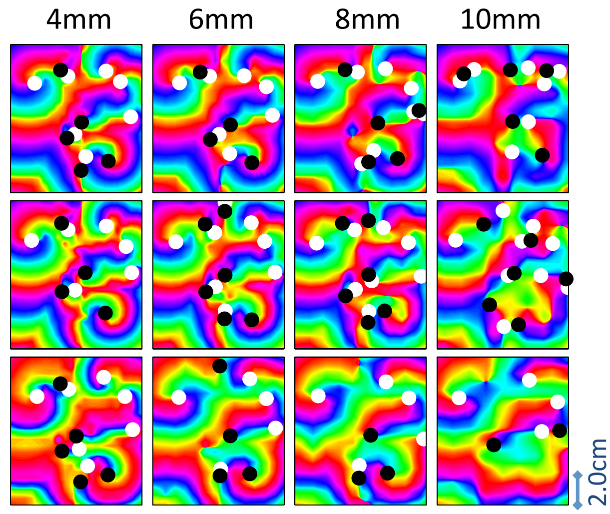

Figure 4. PSs (black and white dots) calculated using AP phase (top), unipolar electrogram phase (middle) and bipolar electrogram phase (bottom) at 4, 6, 8 and 10mm inter-electrode spacings.

Table 1. Error in centre location of isolated rotor and maximum radius of PS trajectory (5.71mm at full-resolution).

	Error in centre location (mm)			Max radius (mm)		
	AP	Unipol	Bipol	AP	Unipol	Bipol
2mm	0.08	0.15	0.13	5.58	5.80	5.64
4mm	0.33	0.83	0.11	5.41	4.03	8.65
6mm	0.59	0.36	0.22	7.54	4.39	5.00
8mm	0.66	0.50	0.83	11.44	5.43	7.45
10mm	1.25	2.11	1.61	14.17	8.18	8.15

Table 2. Framewise mean distance error and standard deviation (mm) for isolated rotor.

	AP	Unipolar	Bipolar
2mm	1.31 ± 0.81	1.57 ± 0.99	2.22 ± 1.08
4mm	2.15 ± 0.96	2.76 ± 1.49	2.68 ± 1.37
6mm	2.64 ± 1.24	3.04 ± 1.50	2.84 ± 1.46
8mm	3.25 ± 1.55	3.42 ± 1.56	2.77 ± 1.43
10mm	3.40 ± 2.11	4.58 ± 2.09	3.92 ± 2.15

The centroid of the trajectory was also calculated. The error in this centroid and the maximum radius of the trajectory, for each datatype and inter-electrode spacing, is given in Table 1. In general for each datatype, the error in the location estimation increased with larger spacing, as expected. The bipolar algorithm generally provided an improved prediction of rotor core location than unipolar data. The maximum radius of the trajectories were larger at the coarser resolutions. In addition, we quantified the error in the isolated rotor PS location on a frame-by-frame basis, shown as mean and standard deviation in Table 2. Error was seen to increase with increasing inter-electrode spacing. The bipolar algorithm provided a slight improvement in its PS location estimate for larger electrode spacings, compared to the unipolar case.

A comparison of the overall distribution of PSs, calculated for each signal type and at each inter-electrode spacing, is shown in Fig. 4. The mean and standard deviation of the number of PSs per frame was 9.62 ± 2.72 for the full resolution AP data; other results are shown in Table 3. At coarser resolutions, both AP and unipolar electrogram data had an increased number of false detections, whilst there were fewer PSs detected per frame for bipolar electrogram phase.

Finally, heat maps were calculated, showing the overall spatial distribution of PSs throughout the simulation. The maps were smoothed with a bin-size of 2mm to reduce artefacts introduced by the use of different inter-electrode spacings. Example heat maps are shown in Fig. 3 and clearly identify the hotspot associated with the isolated rotor. Table 4 shows correlations between each map and the full-resolution map. These again decreased with increasing inter-electrode spacing and were similar between signal types.

4. Discussion

We have presented an approach to identify rotor core locations using phase computed from bipolar electrograms and tested the algorithms on simulated data. Bipolar electrogram phase was observed to be as effective as AP phase for rotor tip detection, and potentially may be used clinically as an alternative method to unipolar electrogram phase to locate rotor PSs in AF. The errors in the centre locations of the isolated rotor are not considered to be of a clinically relevant magnitude, and are significantly less

Table 3. Mean number of PSs per frame.

	AP	Unipolar	Bipolar
2mm	9.45 ± 2.57	9.46 ± 2.81	9.56 ± 2.59
4mm	9.66 ± 2.59	10.06 ± 2.99	9.50 ± 2.62
6mm	9.88 ± 2.59	10.61 ± 2.97	9.27 ± 2.53
8mm	12.27 ± 3.32	11.62 ± 3.52	8.84 ± 2.38
10mm	11.64 ± 2.95	12.11 ± 3.72	8.33 ± 2.41

Table 4. Correlation of PS distribution heat maps with full-resolution AP data heat map.

	AP	Unipolar	Bipolar
2mm	0.91	0.81	0.80
4mm	0.65	0.56	0.60
6mm	0.54	0.66	0.52
8mm	0.48	0.50	0.43
10mm	0.38	0.29	0.29

than the diameter of an ablation catheter. In general, the maximum radius of the bipolar electrogram trajectories are found to be slightly larger than that of unipolar data, although the errors are smaller on a frame-by-frame basis.

Further work will test the methods on bipolar electrogram data acquired from experimental and clinical recordings, to establish if the above conclusions translate to these data.

Acknowledgements

This work was supported by the British Heart Foundation (BHF); grants FS/11/22/28745 & RG/10/11/28457; the ElectroCardioMaths Programme of the Imperial BHF Centre of Research Excellence; the NIHR Imperial Biomedical Research Centre; and an Academy of Medical Sciences Starter Grant (AMS-SGCL8-Ng).

References

[1] Davidenko JM, Kent PF, Chialvo DR, Michaels DC, Jalife J. Sustained vortex-like waves in normal isolated ventricular muscle. Proceedings of the National Academy of Sciences of the United States of America November 1990; 87(22):8785–9.

[2] Allessie Ma, de Groot NMS, Houben RPM, Schotten U, Boersma E, Smeets JL, Crijns HJ. Electropathological substrate of long-standing persistent atrial fibrillation in patients with structural heart disease: longitudinal dissociation. Circulation Arrhythmia and electrophysiology December 2010;3(6):606–15.

[3] Narayan SM, Krummen DE, Rappel WJ. Clinical mapping approach to diagnose electrical rotors and focal impulse sources for human atrial fibrillation. Journal of cardiovascular electrophysiology May 2012;23(5):447–54.

[4] Haissaguerre M, Hocini M, Shah AJ, Derval N, Sacher F, Jais P, Dubois R. Noninvasive panoramic mapping of human atrial fibrillation mechanisms: a feasibility report. Journal of cardiovascular electrophysiology June 2013;24(6):711–7.

[5] Gray R, Pertsov A, Jalife J. Spatial and temporal organization during cardiac fibrillation. Nature 1998;393(May):75–78.

[6] Clayton RH, Zhuchkova Ea, Panfilov aV. Phase singularities and filaments: simplifying complexity in computational models of ventricular fibrillation. Progress in biophysics and molecular biology 2006;90(1-3):378–98.

[7] Nash MP, Mourad A, Clayton RH, Sutton PM, Bradley CP, Hayward M, Paterson DJ, Taggart P. Evidence for multiple mechanisms in human ventricular fibrillation. Circulation August 2006;114(6):536–42.

[8] Courtemanche M, Ramirez RJ, Nattel S. Ionic mechanisms underlying human atrial action potential properties: insights from a mathematical model. The American journal of physiology July 1998;275(1 Pt 2):H301–21.

[9] Courtemanche M, Ramirez RJ, Nattel S. Ionic targets for drug therapy and atrial fibrillation-induced electrical remodeling: insights from a mathematical model. Cardiovascular research May 1999;42(2):477–89.

[10] Pandit SV, Berenfeld O, Anumonwo JMB, Zaritski RM, Kneller J, Nattel S, Jalife J. Ionic determinants of functional reentry in a 2-D model of human atrial cells during simulated chronic atrial fibrillation. Biophysical journal June 2005;88(6):3806–21.

[11] Rush S, Larsen H. A Practical Algorithm for Solving Dynamic Membrane Equations. Biomedical Engineering IEEE Transactions ldots 1978;389–392.

[12] Sato D, Xie LH, Sovari AA, Tran DX, Morita N, Xie F, Karagueuzian H, Garfinkel A, Weiss JN, Qu Z. Synchronization of chaotic early afterdepolarizations in the genesis of cardiac arrhythmias. Proceedings of the National Academy of Sciences of the United States of America 2009; 106:2983–2988.

[13] Ng J, Kadish AH, Goldberger JJ. Effect of electrogram characteristics on the relationship of dominant frequency to atrial activation rate in atrial fibrillation. Heart rhythm the official journal of the Heart Rhythm Society November 2006;3(11):1295–305.

[14] Bray MA, Wikswo J. Considerations in phase plane analysis for nonstationary reentrant cardiac behavior. Physical Review E May 2002;65(5):051902.

[15] Bray MA, Wikswo JP. Use of topological charge to determine filament location and dynamics in a numerical model of scroll wave activity. IEEE transactions on bio medical engineering October 2002;49(10):1086–93.

Address for correspondence:

Caroline H Roney
National Heart and Lung Institute, Imperial College, 4th floor, Imperial Centre for Translational and Experimental Medicine, Hammersmith Campus, Du Cane Road, London W12 0NN, UK.
caroline.roney10 at imperial.ac.uk